Acta Cryst E CRYSTALLOGRAPHIC COMMUNICATIONS

ISSN 2056-9890

Synthesis, crystal structure and Hirshfeld surface of bis(2-aminopyridinium) hexachloridostannate(IV)

Rochdi Ghallab,[a]* Mehdi Boutebdja,[a] George Dénès[b] and Hocine Merazig[a]

[a]Environmental Molecular, and Structural Chemistry Research Unit, University of, Constantine-1, 25000, Constantine, Algeria, and [b]Laboratory of Solid State Chemistry and Mossbauer Spectroscopy, Departement of, Chemistry and Biochemistry, Concordia University, 7141 Sherbrooke St. West, Montreal, H4B 1R6, QC, Canada. *Correspondence e-mail: rochdi.ghallab@gmail.com

Received 1 June 2020
Accepted 9 July 2020

Edited by W. T. A. Harrison, University of Aberdeen, Scotland

Keywords: Zero-dimensional hybrid perovskite; aminopyridine; Hirshfeld surface; Raman spectroscopy; crystal structure.

CCDC reference: 1904730

Supporting information: this article has supporting information at journals.iucr.org/e

In the title molecular salt, $(C_5H_7N_2)_2[SnCl_6]$, the cation is protonated at the pyridine N atom and the complete dianion is generated by a crystallographic centre of symmetry. In the crystal, N—H···Cl hydrogen bonds link the components into a three-dimensional network built up from the stacking of alternate cationic and anionic layers. The nature of the intermolecular interactions has been analysed in terms of the Hirshfeld surfaces of the cations and the anions. The thermal behaviour and the Raman spectrum of the title compound are reported.

1. Chemical context

So-called 'zero-dimensional' hybrid perovskites are characterized by a structure formed by isolated inorganic octahedra (or bioctahedra) and an organic cation (Cheng & Lin, 2010). They are easy to prepare through simple techniques (Mitzi, 2004) and they combine the properties of the various organic and inorganic compounds, *i.e.* the flexibility of the organic part, and the thermal stability and the rigidity of the inorganic part, in a single material, by cooperative effects, to obtain properties that are more than just the sum of the initial properties: an organic/inorganic 'synergy' is created. For example, in these hybrid materials, the organic part can have non-linear optical properties (Bi *et al.*, 2008). Most of the physical properties come from the inorganic part, such as the electronic transport properties, the optical photoluminescence properties (Yangui *et al.*, 2019), or even magnetic properties (Manser *et al.*, 2016). As part of our studies in this area, we now describe the synthesis and structure of the title molecular salt, (I).

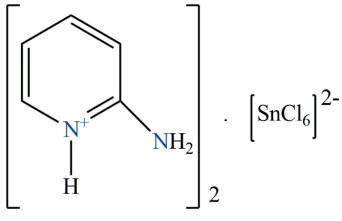

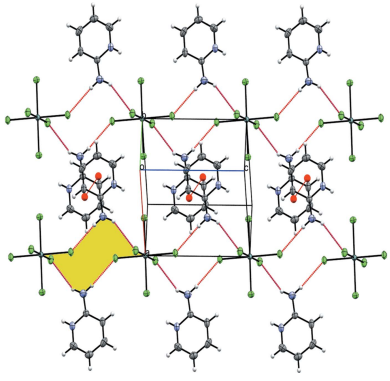

2. Structural commentary

Compound (I) with formula $(C_5H_7N_2)^+_2{\cdot}[SnCl_6]^{2-}$, crystallizes in the triclinic space group $P\overline{1}$ (Fig. 1).

In the synthesis, the oxidation number of tin changes from +2 to +4 such that the resultant tin(IV) atom is hexacoordinated by chlorine atoms, generating a weakly distorted

Table 1
Hydrogen-bond geometry (Å, °).

D—H···A	D—H	H···A	D···A	D—H···A
N1—H1···Cl1^{i}	0.77 (2)	2.79 (3)	3.3155 (18)	128 (3)
N2—H2A···Cl1^{ii}	0.86	2.62	3.406 (2)	152
N2—H2B···Cl2^{iii}	0.86	2.52	3.358 (2)	166

Symmetry codes: (i) $x, y+1, z$; (ii) $-x-1, -y+1, -z$; (iii) $-x-1, -y+1, -z+1$.

octahedron in which the metal ion lies on a crystallographic inversion centre: the length of the Sn—Cl bonds varies from 2.4216 (4) to 2.4474 (5) Å. As for the Cl—Sn—Cl angles, the discrepancy of about ± 1° [89.109 (18)–90.805 (16)°] compared to the 90° value angle of a regular octahedron shows that the angular distortion is very small. These values are comparable to those of the same anion associated with other types of cations (BelhajSalah *et al.*, 2018). The absence of larger distortions can probably be attributed to the fact that the hexachlorostannate(IV) anions are free, *i.e.* none of the chloride ions are bridging although they do accept N—H···Cl hydrogen bonds from the organic cations, which ensures charge balance.

In the pyridinium ring of the cation, the C—C bond lengths vary from 1.328 (3) to 1.405 (3) Å and the C—N bond lengths are 1.341 (3) Å and 1.344 (2) Å. The values of the C—C—C angles in the pyridinium ring vary from 118.9 (2) to 120.9 (2)° whereas the C—N—C angle is 124.30 (18)°: the larger angle can be attributed to the protonation of the N atom. These values are comparable with those of the same cation associated with other types of anions (Rao *et al.*, 2011).

3. Supramolecular features

The special position of tin(IV) in the crystal of (I) gives rise to an alternation of cationic and anionic layers lying parallel to the (001) plane (Fig. 2*a*). The intermolecular interactions in (I) were analysed using *PLATON* (Spek, 2020), which shows that the structural cohesion in the crystalline structure of the compound (I) is ensured by N—H···Cl hydrogen bonds: Fig. 2*a*. The distances and the angles describing these interactions are presented in Table 1.

The combination of N2—H2A···Cl1 and N2—H2B···Cl2 hydrogen bonds generates a chain of rings propagating along the [001] direction with a graph-set pattern of $R_4^4(12)$ (Etter *et al.*, 1990), Fig. 2(*b*). The cohesion between chains is ensured by π-stacking interactions between centrosymmetrically related aromatic rings of the cations: $Cg1\cdots Cg1$ = 3.552 (13) Å; interplanar angle α = 0.0 (11)°; slippage = 1.246 Å. We also note the presence of a Y—$X\cdots Cg1$ type interaction between Sn1—Cl2 and $Cg1$ at an $X\cdots Cg$ distance of 3.6581 (11) Å [Fig. 2(*a*)].

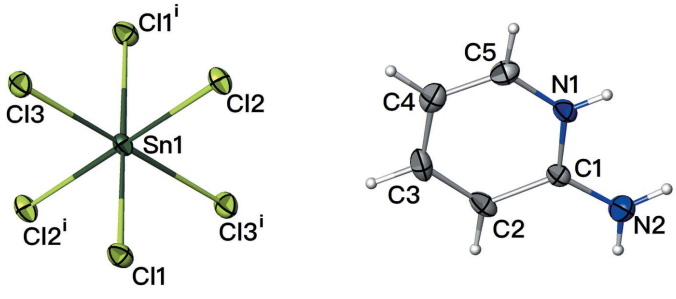

Figure 1
The molecular structure of the title compound with displacement ellipsoids drawn at the 30% probability level [Symmetry code: (i) $-x, -y, -z$].

4. Hirshfeld surface analysis:

To further characterize the intermolecular interactions in (I), the Hirshfeld surface method was used (Spackman & Jayatilaka, 2009). In addition, its two-dimensional fingerprints

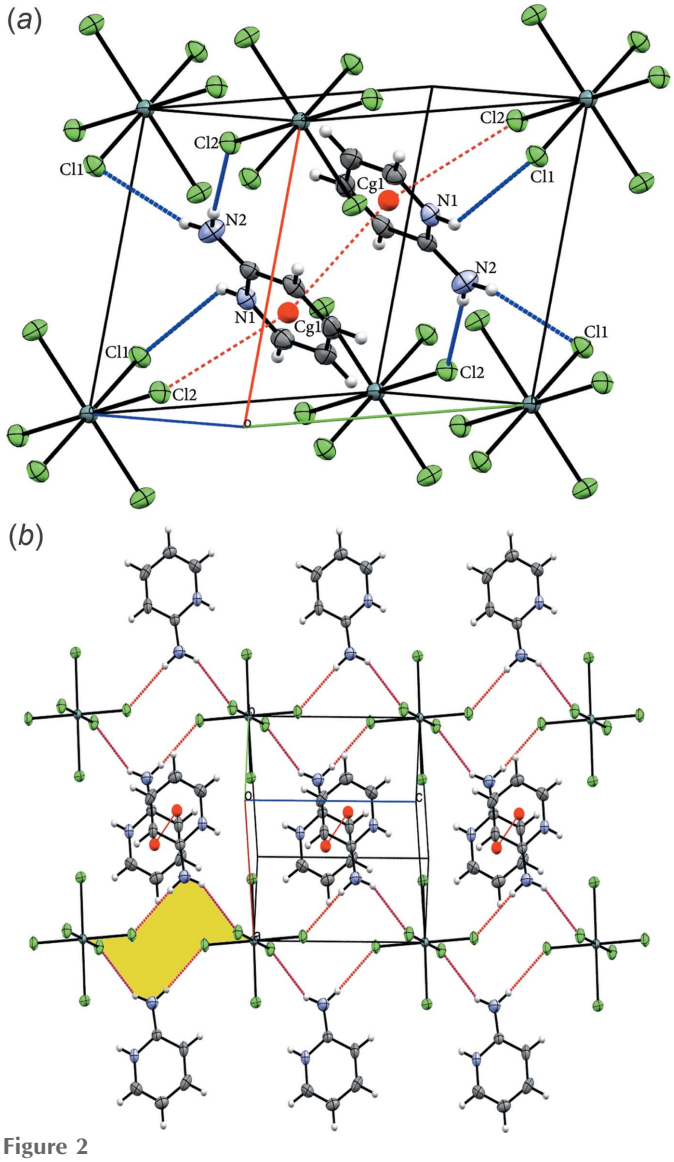

Figure 2
(*a*) Hydrogen bonds [symmetry codes: (i) $x, y+1, z$; (ii) $-x-1, -y+1, -z$; (iii) $-x-1, -y+1, -z+1$] (blue dashed lines), π-stacking interactions (symmetry operation: $-1-x, 1-y, 1-z$) and Y—$X\cdots Cg$ (symmetry operation: $x, -1+y, z$) (red dashed lines) in the unit cell of compound (I). (*b*) A view of the ring motifs along the *c* axis with the strongest hydrogen bonds and π-stacking interactions indicated by red dotted lines.

(Spackman & McKinnon, 2002) were calculated using the program *Crystal Explorer 17* (Turner *et al.*, 2017). The d_{norm} representation mode was used in which red spots identify close contacts; in the white areas, the distance separating the neighboring atoms approaches the sum of the van der Waals radii of the concerned atoms whereas blue areas illustrate areas where neighbouring atoms are too far apart to interact significantly with each other. The presence of the adjacent red and blue triangles, obtained by using the shape index as a representation mode, demonstrates the presence of π–π and Y—X···π type interactions.

The Hirshfeld surface [Fig. 3(*a*)] shows red spots corresponding to H···Cl/Cl···H close contacts, which are due to the N—H···Cl hydrogen bonds. The presence of the adjacent red and blue triangles in Fig. 3(*b*) demonstrates the presence of the *Cg*1···*Cg*1 and Sn—Cl2···*Cg*1 interactions. The contribution of different kinds of interatomic contacts to the Hirshfeld surfaces of the individual cations and anions is shown in the fingerprint plots in Fig. 4 and Fig. 5, respectively. These interactions are ensured by 47.3% of hydrogen bonds (H···Cl), 3.2% of Y—X··· type (N···Cl and C···Cl), 6.6% of π–π stacking type (C···C and C···N/N···C), 15.6% of C—H···π type (C···H/H···C), 6.2% of N—H···π type (N···H/H···N) and 21.1% of H···H van der Waals interactions. The two-dimensional fingerprint analysis for the anionic moieties

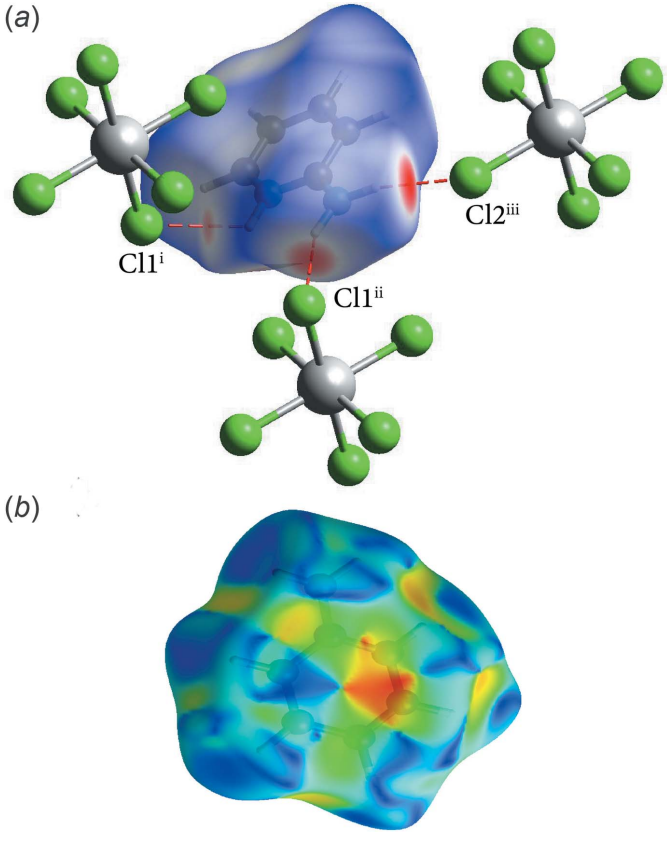

Figure 3
(*a*) A view of the Hirshfeld surface mapped over d_{norm} for compound (I) in the range −0.3387 to +1.0913 arbitrary units, highlighting the N—H···Cl interactions and (*b*) the Hirshfeld surface of the cation mapped over shape-index in the range −1.00 to +1.00 arbitrary units.

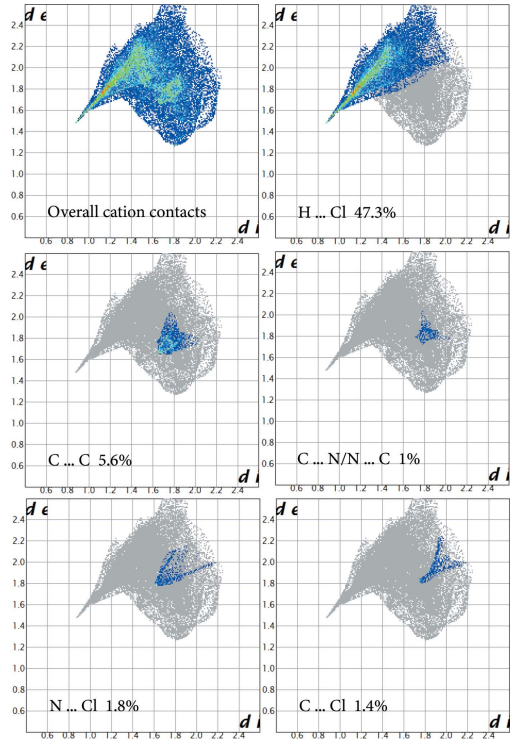

Figure 4
Two-dimensional fingerprint plots for the cation of the title compound, and delineated into the principal contributions of H···Cl, C···C, C···N/N···C, N···Cl and C···Cl contacts. Other significant contacts are H···H (21.1%), H···C/C···H (15.6%) and H···N/N···H (6.2%).

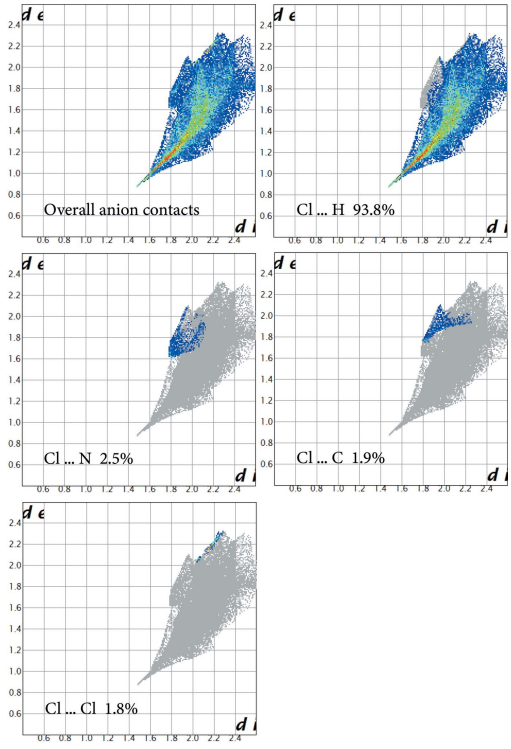

Figure 5
Two-dimensional fingerprint plots for the anion of the title compound, and those delineated into the principal contributions of Cl···H, Cl···C, Cl···N and Cl···Cl contacts.

reveals that hydrogen bonds (Cl···H) represent 93.8%, Y—X···π type interactions represent 4.4% (Cl···N and Cl···C) and van der Waals interactions of the Cl···Cl type represent 1.8% of the surface contacts.

5. Database survey

A search of the Cambridge Structural Database (CSD Version 5.41; Groom *et al.*, 2016) for structures similar to (I) gave several compounds such as 2-aminopyridinium hexachlorobismuth(III) (Rao *et al.*, 2011), 2-aminopyridinium hexachloroindium(III) (Jin *et al.*, 2011), 4-aminopyridinium hexachloroantimonate(V) (Kulicka *et al.*, 2006) and 4-aminopyridinium hexachlorostannate(IV) (Rademeyer *et al.*, 2007) among others, but the last of these (refcode RIGDER) is of particular interest: RIGDER and (I) both crystallize in space group $P\overline{1}$ where the $[SnCl_6]^{2-}$ anions are associated with special positions and an organic–inorganic layered structure lying parallel to the (001) plane results.

Crystalline cohesion in RIGDER and (I) is ensured by dipole–dipole interactions and hydrogen bonds of the N—H···Cl type with a slight difference in the donor–acceptor angles and distances of the two compounds. The different arrangement of the nitrogen atoms in the cation in RIGDER leads to much weaker π–π stacking compared to (I): the centroid separations are 4.24 (1) and 3.552 (13) Å, respectively. We also notice a slight difference between the two compounds in the interaction percentages calculated by the Hirshfeld surface analysis (see Table S1 in the supporting information).

6. Thermal analysis

In order to investigate the thermal stability of (I), thermogravimetric analysis (DTA/TGA) was performed under an N_2 atmosphere at a heating rate of 10°C min^{-1} in the temperature range from 25 to 500°C. The thermogram of (I) (see Fig. S2 in the supporting information) shows that the compound loses 64.4% of its mass in the temperature range of 270–304°C. The mass loss can be attributed to the degradation of the organic entity and two chlorine atoms (Janiak & Blazejowski, 1990) to leave a reside of $SnCl_4$.

7. Synthesis and crystallization

Tin(II) chloride dihydrate (2.25 mmol) was mixed with 2-aminopyridine (0.94 mmol) and a few drops of hydrochloric acid in an aliquot of distilled water in 1:1 molar ratio was added. After stirring, the mixture was poured into a vial (biotage microwave vial 2–5 ml) that was put in an oven for three days at 393 K. Upon cooling, prism-shaped crystals of (I) were obtained and separated using an optical microscope. ^{1}H NMR (δ ppm), 400 MHz, $CDCl_3$): 8.16 (*br s*, 2H, NH_2), 7.95–7.89 (*m*, 2H CH Py), 7.03 (*d*, J_{HH} = 8.9 Hz,1H CH Py), 6.84 (*t*, J_{HH} = 6.6 Hz, 1H CH Py). ^{13}C NMR (δ ppm), 125 MHz, $CDCl_3$): 154.6 (quat C Py), 144.4 (CH Py), 136.1 (CH Py), 113.8 (CH Py), 112.5 (CH Py).

Table 2
Experimental details.

Crystal data	
Chemical formula	$(C_5H_7N_2)_2[SnCl_6]$
M_r	521.64
Crystal system, space group	Triclinic, $P\overline{1}$
Temperature (K)	298
a, b, c (Å)	7.4537 (1), 8.0674 (1), 8.1025 (1)
α, β, γ (°)	83.791 (1), 82.591 (1), 71.407 (1)
V (Å^3)	456.77 (1)
Z	1
Radiation type	Mo $K\alpha$
μ (mm^{-1})	2.27
Crystal size (mm)	0.08 × 0.08 × 0.07
Data collection	
Diffractometer	Bruker SMART APEXII area detector
Absorption correction	Multi-scan (*SADABS*; Bruker, 2016)
T_{min}, T_{max}	0.834, 0.853
No. of measured, independent and observed [$I > 2\sigma(I)$] reflections	10455, 2011, 1910
R_{int}	0.021
(sin $\theta/\lambda)_{max}$ (Å^{-1})	0.641
Refinement	
$R[F^2 > 2\sigma(F^2)]$, $wR(F^2)$, S	0.017, 0.037, 1.06
No. of reflections	2011
No. of parameters	101
No. of restraints	36
H-atom treatment	H atoms treated by a mixture of independent and constrained refinement
$\Delta\rho_{max}$, $\Delta\rho_{min}$ (e Å^{-3})	0.56, −0.34

Computer programs: *APEX2* and *SAINT* (Bruker, 2016), *SIR2004* (Burla *et al.*, 2007), *SHELXL* (Sheldrick, 2015) and *OLEX2* (Dolomanov *et al.*, 2009).

The raman spectrum for (I) (Fig. 6) was recorded in the frequency range 4000–60 cm^{-1}. The Py, ν, δ, γ and τ are: pyridine ring, stretching, in-plane bending, out-of-plane bending and torsion, respectively. RS (cm^{-1}): 3334 ν(N—H), 3215 ν (N—H), 3106 ν(C—H), 1657 ν(py)+δ(N—H)+δ(NH_2), 1620 ν(py), 1542 ν(py), 1472 ν(py)+δ(C—H), 1412 ν(py)+δ(C—H), 1378 ν(py)+δ(C—H), 1324 ν(py)+δ(C—H), 1239 ν(py)+δ(C—H), 1164 δ(py)+δ(C—H), 1120 δ(py)+δ(C—H), 996 δ(py), 846 Pyridine ring breathing+γ(C—H), 623 γ(py), 551 γ(py), 406 γ(py), 384 γ(py), 305 ν_1 (Sn—Cl), 216 ν_2 (Sn—Cl), 106 τ(py)+ ν(N—H···Cl) (Shaw *et al.*, 1988; Ureña *et al.*, 2003; Cook, 1961).

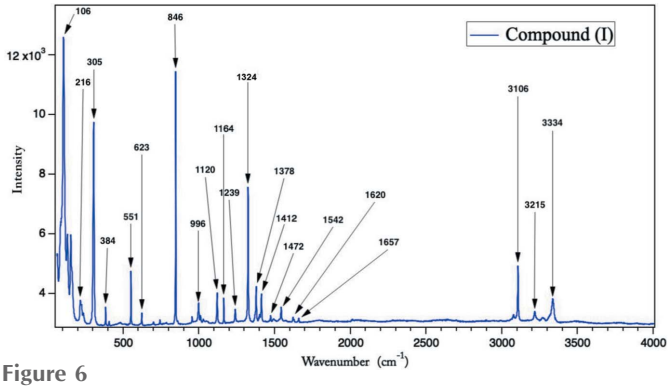

Figure 6
Raman spectrum of compound (I).

8. Refinement

Crystal data, data collection and structure refinement details are summarized in Table 2. The C-bound H atoms and the anine H atom were placed geometrically and refined as riding atoms [C—H = 0.93 Å and U_{iso}(H) = 1.2U_{eq}(C)]; the pyridine N—H atom was located in a difference map and its position was freely refined.

Acknowledgements

Thanks are due to Jean-Claude Daran, Eric Manoury, Eric Deydier and Gabor Molnar from LCC Toulouse France for their technical support.

Funding information

Funding for this research was provided by: Unité de Recherche de Chimie de l'Environnement, Moléculaire et Structurale (UR.CHEMS); Direction Générale de la Recherche Scientifique et du Développement Technologique.

References

BelhajSalah, S., Abdelbaky, M. S. M., García-Granda, S., Essalah, K., Ben Nasr, C. & Mrad, M. L. (2018). *Solid State Sci.* **86**, 77–85.

Bi, W., Louvain, N., Mercier, N., Luc, J., Rau, I., Kajzar, F. & Sahraoui, B. (2008). *Adv. Mater.* **20**, 1013–1017.

Bruker (2016). *APEX2*, *SAINT* and *SADABS*. Bruker AXS Inc., Madison, Wisconsin, USA.

Burla, M. C., Caliandro, R., Camalli, M., Carrozzini, B., Cascarano, G. L., De Caro, L., Giacovazzo, C., Polidori, G., Siliqi, D. & Spagna, R. (2007). *J. Appl. Cryst.* **40**, 609–613.

Cheng, Z. & Lin, J. (2010). *CrystEngComm*, **12**, 2646–2662.

Cook, D. (1961). *Can. J. Chem.* **39**, 2009–2024.

Dolomanov, O. V., Bourhis, L. J., Gildea, R. J., Howard, J. A. K. & Puschmann, H. (2009). *J. Appl. Cryst.* **42**, 339–341.

Etter, M. C., MacDonald, J. C. & Bernstein, J. (1990). *Acta Cryst.* B**46**, 256–262.

Groom, C. R., Bruno, I. J., Lightfoot, M. P. & Ward, S. C. (2016). *Acta Cryst.* B**72**, 171–179.

Janiak, T. & Blazejowski, J. (1990). *Thermochim. Acta*, **157**, 137–154.

Jin, X.-D., Sun, L.-C., Wang, H.-B. & Ge, C.-H. (2011). *Acta Cryst.* E**67**, m1602.

Kulicka, B., Jakubas, R., Pietraszko, A., Medycki, W. & Świergiel, J. (2006). *J. Mol. Struct.* **783**, 88–95.

Manser, J. S., Christians, J. A. & Kamat, P. V. (2016). *Chem. Rev.* **116**, 12956–13008.

Mitzi, D. B. (2004). *J. Mater. Chem.* **14**, 2355–2365.

Rademeyer, M., Lemmerer, A. & Billing, D. G. (2007). *Acta Cryst.* C**63**, m289–m292.

Rao, A. S., Baruah, U. & Das, S. K. (2011). *Inorg. Chim. Acta*, **372**, 206–212.

Shaw, R. A., Castro, C., Dutler, R., Rauk, A. & Wieser, H. (1988). *J. Chem. Phys.* **89**, 716–731.

Sheldrick, G. M. (2015). *Acta Cryst.* C**71**, 3–8.

Spackman, M. A. & Jayatilaka, D. (2009). *CrystEngComm*, **11**, 19–32.

Spackman, M. A. & McKinnon, J. J. (2002). *CrystEngComm*, **4**, 378–392.

Spek, A. L. (2020). *Acta Cryst.* E**76**, 1–11.

Turner, M. J., Mckinnon, J. J., Wolff, S. K., Grimwood, D. J., Spackman, P. R., Jayatilaka, D. & Spackman, M. A. (2017). *Crystal Explorer 17*. The University of Western Australia.

Ureña, F. P., Gómez, M. F., González, J. J. L. & Torres, E. M. (2003). *Spectrochim. Acta A Mol. Biomol. Spectrosc.* **59**, 2815–2839.

Yangui, A., Roccanova, R., Wu, Y., Du, M.-H. & Saparov, B. (2019). *J. Phys. Chem. C*, **123**, 22470–22477.

supporting information

Acta Cryst. (2020). E**76**, 1279-1283 [https://doi.org/10.1107/S205698902000941X]

Synthesis, crystal structure and Hirshfeld surface of bis(2-aminopyridinium) hexachloridostannate(IV)

Rochdi Ghallab, Mehdi Boutebdja, George Dénès and Hocine Merazig

Computing details

Data collection: *APEX2* (Bruker, 2016); cell refinement: *SAINT* (Bruker, 2016); data reduction: *SAINT* (Bruker, 2016); program(s) used to solve structure: *SIR2004* (Burla *et al.*, 2007); program(s) used to refine structure: *SHELXL* (Sheldrick, 2015); molecular graphics: *OLEX2* (Dolomanov *et al.*, 2009); software used to prepare material for publication: *OLEX2* (Dolomanov *et al.*, 2009).

Bis(2-aminopyridinium) hexachloridostannate(IV)

Crystal data

$2C_5H_7N_2^+\cdot Cl_6Sn^{2-}$
M_r = 521.64
Triclinic, $P\overline{1}$
a = 7.4537 (1) Å
b = 8.0674 (1) Å
c = 8.1025 (1) Å
α = 83.791 (1)°
β = 82.591 (1)°
γ = 71.407 (1)°
V = 456.77 (1) Å^3
Z = 1
$F(000)$ = 254
D_x = 1.896 Mg m^{-3}
Mo $K\alpha$ radiation, λ = 0.71073 Å
Cell parameters from 1910 reflections
θ = 3.6–27.1°
μ = 2.27 mm^{-1}
T = 298 K
Prism, colourless
0.08 × 0.08 × 0.07 mm

Data collection

Bruker SMART APEXII area detector diffractometer
Radiation source: microfocus sealed X-ray tube, Incoatec Iμs
Mirror optics monochromator
Detector resolution: 7.9 pixels mm^{-1}
ω and φ scans
Absorption correction: multi-scan (SADABS; Bruker, 2016)
T_{min} = 0.834, T_{max} = 0.853
10455 measured reflections
2011 independent reflections
1910 reflections with $I > 2\sigma(I)$
R_{int} = 0.021
θ_{max} = 27.1°, θ_{min} = 3.6°
h = −9→9
k = −10→10
l = −10→10

Refinement

Refinement on F^2
Least-squares matrix: full
$R[F^2 > 2\sigma(F^2)]$ = 0.017
$wR(F^2)$ = 0.037
S = 1.06
2011 reflections
101 parameters
36 restraints
Primary atom site location: structure-invariant direct methods
Hydrogen site location: mixed
H atoms treated by a mixture of independent and constrained refinement
$w = 1/[\sigma^2(F_o^2) + (0.0121P)^2 + 0.2078P]$ where $P = (F_o^2 + 2F_c^2)/3$
$(\Delta/\sigma)_{max} < 0.001$

$\Delta\rho_{max}$ = 0.56 e Å^{-3} $\Delta\rho_{min}$ = −0.33 e Å^{-3}

Special details

Geometry. All esds (except the esd in the dihedral angle between two l.s. planes) are estimated using the full covariance matrix. The cell esds are taken into account individually in the estimation of esds in distances, angles and torsion angles; correlations between esds in cell parameters are only used when they are defined by crystal symmetry. An approximate (isotropic) treatment of cell esds is used for estimating esds involving l.s. planes.

Fractional atomic coordinates and isotropic or equivalent isotropic displacement parameters (Å²)

	x	*y*	*z*	U_{iso}*/U_{eq}
Sn1	0.000000	0.000000	0.000000	0.03137 (6)
Cl3	−0.29282 (7)	0.24458 (7)	−0.00146 (6)	0.04838 (12)
Cl1	−0.17021 (7)	−0.18776 (7)	−0.08097 (6)	0.04442 (11)
Cl2	−0.07788 (7)	−0.07356 (7)	0.29243 (5)	0.04473 (12)
C1	−0.4688 (3)	0.7533 (2)	0.4088 (2)	0.0364 (4)
C2	−0.4174 (3)	0.6744 (3)	0.5662 (2)	0.0455 (5)
H2	−0.481358	0.726282	0.663052	0.055*
C3	−0.2718 (3)	0.5200 (3)	0.5747 (3)	0.0538 (6)
H3	−0.237750	0.465902	0.678377	0.065*
C4	−0.1736 (3)	0.4425 (3)	0.4298 (3)	0.0540 (5)
H4	−0.075494	0.337051	0.436149	0.065*
C5	−0.2228 (3)	0.5220 (3)	0.2827 (3)	0.0498 (5)
H5	−0.157176	0.473379	0.184945	0.060*
N1	−0.3668 (3)	0.6723 (2)	0.2748 (2)	0.0414 (4)
N2	−0.6083 (3)	0.9016 (2)	0.3872 (3)	0.0568 (5)
H2A	−0.633148	0.945458	0.288064	0.068*
H2B	−0.674139	0.954202	0.472330	0.068*
H1	−0.397 (4)	0.716 (3)	0.189 (3)	0.061 (8)*

Atomic displacement parameters (Å²)

	U^{11}	U^{22}	U^{33}	U^{12}	U^{13}	U^{23}
Sn1	0.02900 (9)	0.04010 (10)	0.02432 (9)	−0.01029 (7)	−0.00234 (6)	−0.00090 (6)
Cl3	0.0391 (2)	0.0533 (3)	0.0432 (3)	0.0020 (2)	−0.0084 (2)	−0.0073 (2)
Cl1	0.0495 (3)	0.0531 (3)	0.0382 (2)	−0.0260 (2)	−0.0058 (2)	−0.0026 (2)
Cl2	0.0467 (3)	0.0600 (3)	0.0261 (2)	−0.0177 (2)	0.00014 (18)	0.00261 (19)
C1	0.0335 (9)	0.0424 (10)	0.0374 (9)	−0.0171 (8)	−0.0039 (7)	−0.0036 (8)
C2	0.0521 (12)	0.0664 (13)	0.0283 (9)	−0.0338 (11)	−0.0015 (8)	−0.0027 (8)
C3	0.0577 (13)	0.0643 (14)	0.0501 (12)	−0.0345 (12)	−0.0251 (10)	0.0215 (10)
C4	0.0444 (12)	0.0477 (12)	0.0717 (15)	−0.0166 (10)	−0.0112 (10)	0.0014 (10)
C5	0.0458 (11)	0.0468 (12)	0.0570 (13)	−0.0158 (10)	0.0039 (10)	−0.0114 (10)
N1	0.0500 (10)	0.0482 (10)	0.0288 (8)	−0.0199 (8)	−0.0027 (7)	−0.0015 (7)
N2	0.0529 (11)	0.0540 (11)	0.0573 (11)	−0.0035 (9)	−0.0117 (9)	−0.0105 (9)

Geometric parameters (Å, º)

Sn1—Cl3^{i}	2.4315 (5)	C2—C3	1.369 (3)
Sn1—Cl3	2.4315 (5)	C3—H3	0.9300

Sn1—Cl1	2.4474 (4)	C3—C4	1.397 (3)
Sn1—Cl1^{i}	2.4474 (4)	C4—H4	0.9300
Sn1—Cl2^{i}	2.4216 (4)	C4—C5	1.328 (3)
Sn1—Cl2	2.4216 (4)	C5—H5	0.9300
C1—C2	1.405 (3)	C5—N1	1.341 (3)
C1—N1	1.344 (2)	N1—H1	0.77 (2)
C1—N2	1.324 (3)	N2—H2A	0.8600
C2—H2	0.9300	N2—H2B	0.8600
Cl3^{i}—Sn1—Cl3	180.0	C1—C2—H2	120.6
Cl3^{i}—Sn1—Cl1	90.889 (18)	C3—C2—C1	118.89 (19)
Cl3—Sn1—Cl1^{i}	90.891 (18)	C3—C2—H2	120.6
Cl3—Sn1—Cl1	89.109 (18)	C2—C3—H3	119.6
Cl3^{i}—Sn1—Cl1^{i}	89.111 (18)	C2—C3—C4	120.85 (19)
Cl1^{i}—Sn1—Cl1	180.0	C4—C3—H3	119.6
Cl2—Sn1—Cl3^{i}	89.575 (17)	C3—C4—H4	120.6
Cl2^{i}—Sn1—Cl3^{i}	90.425 (17)	C5—C4—C3	118.9 (2)
Cl2^{i}—Sn1—Cl3	89.575 (17)	C5—C4—H4	120.6
Cl2—Sn1—Cl3	90.425 (17)	C4—C5—H5	119.9
Cl2—Sn1—Cl1	90.805 (16)	C4—C5—N1	120.1 (2)
Cl2^{i}—Sn1—Cl1^{i}	90.804 (16)	N1—C5—H5	119.9
Cl2^{i}—Sn1—Cl1	89.196 (16)	C1—N1—H1	116.4 (19)
Cl2—Sn1—Cl1^{i}	89.195 (16)	C5—N1—C1	124.30 (18)
Cl2^{i}—Sn1—Cl2	180.0	C5—N1—H1	119.3 (19)
N1—C1—C2	116.94 (18)	C1—N2—H2A	120.0
N2—C1—C2	123.55 (18)	C1—N2—H2B	120.0
N2—C1—N1	119.50 (18)	H2A—N2—H2B	120.0

Symmetry code: (i) −*x*, −*y*, −*z*.

Hydrogen-bond geometry (Å, º)

D—H···*A*	*D*—H	H···*A*	*D*···*A*	*D*—H···*A*
N1—H1···Cl1^{ii}	0.77 (2)	2.79 (3)	3.3155 (18)	128 (3)
N2—H2*A*···Cl1^{iii}	0.86	2.62	3.406 (2)	152
N2—H2*B*···Cl2^{iv}	0.86	2.52	3.358 (2)	166

Symmetry codes: (ii) *x*, *y*+1, *z*; (iii) −*x*−1, −*y*+1, −*z*; (iv) −*x*−1, −*y*+1, −*z*+1.